

Article

Low-Temperature CO Oxidation over CuO-CeO₂/Fe₂O₃ Catalyst: Effect of KMnO₄ Modification

Lu Feng¹, Xiangdong Xing^{2,*}, Yueli Du², Zhenghua Shen², Hui Zhang¹, Liu Yang¹ and Ming Lv²¹ Xi'an University of Architecture and Technology Huaqing College, Xi'an 710043, China² School of Metallurgical Engineering, Xi'an University of Architecture and Technology, Xi'an 710055, China

* Correspondence: xaxxd@xauat.edu.cn

Abstract: In this paper, the effect of KMnO₄ modification on the performance of CO oxidation over a CuCeO_x/Fe₂O₃ catalyst in industrial flue gas was studied. X-ray diffraction (XRD), scanning electron microscopy (SEM), temperature-programmed reduction by H₂ (H₂-TPR), Fourier transform infrared spectroscopy (FTIR), and Raman spectra were employed to reveal the relationship between the structural properties and the performance of the catalyst. The results show that the catalytic activity could be increased by KMnO₄ modification. CuCeO_x/Fe₂O₃ modified with 0.07 mol/L KMnO₄ exhibited high activity, with a CO conversion of 78.2% at 160 °C. The modification of KMnO₄ reduced the grain size and promoted the uniform dispersion of active particles. In addition, the number of oxygen-containing functional groups increased, which could anchor metal particles and provide active oxygen species for CO oxidation.

Keywords: CuO-CeO₂/Fe₂O₃; low temperature; CO oxidation; KMnO₄ modification



Citation: Feng, L.; Xing, X.; Du, Y.; Shen, Z.; Zhang, H.; Yang, L.; Lv, M. Low-Temperature CO Oxidation over CuO-CeO₂/Fe₂O₃ Catalyst: Effect of KMnO₄ Modification. *Metals* **2023**, *13*, 186. <https://doi.org/10.3390/met13020186>

Academic Editors: Noé Cheung and Yoshitsugu Kojima

Received: 28 November 2022

Revised: 26 December 2022

Accepted: 10 January 2023

Published: 17 January 2023



Copyright: © 2023 by the authors. Licensee MDPI, Basel, Switzerland. This article is an open access article distributed under the terms and conditions of the Creative Commons Attribution (CC BY) license (<https://creativecommons.org/licenses/by/4.0/>).

1. Introduction

In industrial production, the combustion of fossil-fuel-generated flue gas contains a certain amount of CO, which is harmful to both mammals and plants [1,2]. With environmental protection policies becoming increasingly stricter, it is important to find a way to eliminate CO. The catalytic oxidation of CO to nontoxic CO₂ is gaining increasingly more attention due to its simple operation and low energy consumption. Precious metal catalysts, such as Au, have high catalytic activity for CO oxidation [3,4]. However, this process is also limited by the fact that it is difficult to apply it to the removal of CO from industrial flue gas.

Transition metals and rare-earth oxides have a certain low-temperature activity for CO, and the development of high-performance non-precious metal catalysts for industrial flue gas CO treatment has become a hot topic in recent years [5–7]. Among them, the unique reverse II bond of CuO has been found to be beneficial for the adsorption and activation of CO, while CeO₂ and Fe₂O₃ have excellent oxygen storage and release capacities and redox performance, which can provide reactive oxygen species for CO oxidation [8–12]. Cu-Ce/Fe₂O₃ catalysts have shown high low-temperature catalytic activity, making them the most likely replacements of precious metal catalysts at present [13–17]. However, the active particles of Cu-Ce/Fe₂O₃ catalysts tend to sinter easily during application, resulting in a decrease in catalytic activity. Therefore, it is necessary to suppress the aggregation and growth of Cu-Ce/Fe₂O₃ catalysts.

Studies have shown that modifying the catalyst could inhibit the sintering of active particles and improve their dispersibility. Shang et al. [18]. proposed the modification of a Co₃O₄-CeO₂ catalyst with formic acid. After modification, the pore structure and active sites of the catalyst increased, and 100% CO conversion was achieved at 150 °C. Tian et al. [19]. modified a Fe₂O₃/activated carbon (AC) catalyst with KMnO₄, which enriched the oxygen-containing functional groups on the catalyst, increased support defects,

and made the Fe species uniformly dispersed on the surface. Wang et al. [20]. reported that KMnO_4 -modified Fe/CNTs exhibited higher activity and better stability, which could be due to small nanoparticles and weak carrier–metal interactions. However, the effect of the KMnO_4 modification on the Cu-Ce/ Fe_2O_3 catalyst is still unclear.

In the present work, the modification of a Cu-Ce/ Fe_2O_3 catalyst with KMnO_4 was proposed to catalyze CO oxidation at a low temperature. The mechanism by which KMnO_4 affected the performance was studied, which provided ideas for the development of high-performance non-precious metal industrial flue gas CO treatment catalysts.

2. Experiment

2.1. Raw Materials

The names and the purities of the reagents used in the experiment are shown in Table 1, and the experimental equipment and devices are shown in Table 2.

Table 1. Main reagents used in the experiment.

| Reagent | Chemical Formula | Remarks |
|------------------------|--|----------------------------------|
| Cerium nitrate | $\text{Ce}(\text{NO}_3)_3 \cdot 6\text{H}_2\text{O}$ | Analytical-grade reagent |
| Copper nitrate | $\text{Cu}(\text{NO}_3)_2 \cdot 3\text{H}_2\text{O}$ | Analytical-grade reagent |
| Ferric nitrate | $\text{Fe}(\text{NO}_3)_3 \cdot 9\text{H}_2\text{O}$ | Analytical-grade reagent |
| Ammonia | $\text{NH}_3 \cdot \text{H}_2\text{O}$ | Analytical-grade reagent |
| Nitric acid | HNO_3 | Analytical-grade reagent |
| Sulfuric acid | H_2SO_4 | Analytical-grade reagent |
| Potassium permanganate | KMnO_4 | Analytical-grade reagent |
| Polyvinyl alcohol | $\text{C}_2\text{H}_4\text{O}_n$ | Analytical-grade reagent |
| Potassium bromide | KBr | Analytical-grade reagent |
| Nitrogen | N_2 | High-purity gas (99.9%) |
| Oxygen | O_2 | High-purity gas (99.9%) |
| Sulfur dioxide | SO_2 | $\text{N}_2\text{-SO}_2$ (1.05%) |
| Carbon monoxide | CO | $\text{N}_2\text{-CO}$ (1.03%) |

Table 2. Instruments and equipment used in the experiment.

| Name | Model |
|---|----------------------|
| Electronic analytical balance | AL204 |
| Electric blast-drying oven | DZF-6020A |
| Magnetic stirrer | DF101-S |
| Constant-temperature water bath | THZ-82 |
| Vacuum tube furnace | GSL-1400X |
| X-ray photoelectron spectrometer | Thermo ESCALAB 250XI |
| X-ray diffractometer | D8 ADVANCE A25 |
| Scanning electron microscope | VEGA 3 XMU/XMH |
| Fourier transform infrared spectroscopy | Nexus870 |
| Chemisorber | AutoChem II 2920 |
| Confocal laser Raman spectrometer | LabRAM HR |
| Pore size analyzer | JW-BK222 |

It can be seen in Table 1 that all raw materials were of pure reagent grade and that the gas was a high-purity gas, which could allow for experimental errors to be avoided and guarantee the accuracy of the experimental results.

Table 2 presents all the experimental instruments used in this work to complete the catalyst preparation and characterization.

2.2. Catalyst Preparation

2.2.1. Load Material Pretreatment

Fe_2O_3 : Dissolve 4 g of ferric nitrate in deionized water, add excess ammonia water under stirring to obtain precipitation, adjust the pH of the solution to 9.0, stir magnetically

for 1 h, then perform suction filtration, and rinse with deionized water until neutral. After drying at 80 °C for 8 h, the solid was calcined at 400 °C for 4 h in an air atmosphere to obtain the product Fe₂O₃.

2.2.2. Modified Potassium Permanganate

Fe₂O₃ composites with a mass of 4 g were added to 200 mL of a potassium permanganate aqueous solution at a range of concentrations, namely, 0.03 mol/L, 0.05 mol/L, 0.07 mol/L, and 0.09 mol/L. The solution was magnetically stirred at 70 °C for 30 min, filtered, and washed until the filtrate was nearly colorless. The treated Fe₂O₃ was recorded as 3K/Fe₂O₃, 5K/Fe₂O₃, 7K/Fe₂O₃, and 9K/Fe₂O₃, respectively.

2.2.3. Supported Copper Cerium

During the impregnation process, an aqueous solution of copper nitrate and cerium nitrate was used to dissolve Cu/Ce at a molar ratio of 1:1 in a certain amount of distilled water, and the total weight of the metal oxides was controlled to be 10 wt%. After impregnation, the samples were magnetically stirred at room temperature for 8 h, then dried at 120 °C for 12 h, and subsequently calcined at 300 °C under a N₂ atmosphere for 3 h. The obtained catalysts denoted as CuCeO_{x-x}K/Fe₂O₃ catalysts were prepared in the same way.

2.3. Catalyst Characterization

2.3.1. Powder X-Ray Diffraction (XRD)

The phase structure of the catalyst was detected using a D8 ADVANCE A25 diffractometer on the instrument-sharing platform of Xi'an University of Architecture and Technology. The scan range was 2θ (5–70°), with Cu Kα radiation (λ = 0.154 nm) at a scan rate of 6°/min.

The microscopic topography of the catalyst was collected by using a VEGA 3 XMU/XMH scanning electron microscope (CIQTEK, Hefei, China). A small number of catalyst samples were evenly dispersed on the surface of a conductive adhesive and fixed on the sample stage for gold spraying to obtain high-quality scanning electron microscope images.

2.3.2. N₂ Adsorption/Desorption

The pore structure characteristics of the catalyst samples were measured by using a JW-BK222 physical adsorption analyzer. The samples were degassed at 300 °C for 3 h before the experiment, and N₂ adsorption/desorption experiments were carried out at liquid nitrogen temperature (−197 °C). The specific surface area of the catalyst was calculated by using the BET (Brunauer-Emmett-Teller) equation, and the pore size distribution and total pore volume of the catalyst were analyzed by using the BJH (Barrett-Joyner-Halenda) method.

2.3.3. Temperature-Programmed Reduction and Desorption

Temperature-programmed reduction and desorption (H₂-TPR and CO-TPD, respectively) were determined using an AutoChem II model 2920 instrument (One Micromeritics Drive, Norcross, GA, USA). The mass of the catalyst sample was 50 mg. First, the catalyst sample was placed in a nitrogen atmosphere at 300 °C for 1 h to desorb the gas on the catalyst surface. On this basis, the sample was cooled to room temperature, the gas was adjusted to a 10% H₂/Ar mixture with a gas flow rate of 50 mL/min, and the temperature was increased to 900 °C at a heating rate of 10 °C/min. Temperature-programmed desorption was performed to adjust the gas to a 10% CO/Ar mixture, and the remaining steps were the same.

2.3.4. Fourier Transform Infrared Spectroscopy (FT-IR)

The surface functional groups of the catalysts were measured using a Nexus 870 spectrometer (Nicolet, Beijing, China). The steps were as follows: First, samples of the same mass were mixed and ground with KBr according to a mass ratio of 1:200, and then the

mixture of the same mass (50 mg) was formed into a sheet under a pressure of 10 MPa for infrared testing. The measurement range was 500–4000 cm^{-1} .

2.3.5. Raman Spectroscopy (Raman)

The Raman spectrum was tested on the instrument sharing platform of Xi'an University of Architecture and Technology, using a LabRAM HR micro-confocal laser Raman spectrometer with a spectral scanning range of 200–2000 cm^{-1} .

2.4. Catalytic Activity Measurement

The catalyst activity test was performed on a fixed flow bed equipped with an 8 mm quartz tube. For each test, 400 mg of the catalyst was taken. The reaction temperature was heated from 80 °C to 160 °C at a heating rate of 5 °C/min. The conversion rate of CO was tested at 10 °C as an interval point, and each temperature point waited for the concentration of CO to remain stable for 30 min before heating up to the next point. The CO conversion rate was calculated by using the following formula:

$$X_{CO} = \left(1 - \frac{CO_{out}}{CO_{in}}\right) \times 100\% \quad (1)$$

where CO_{in} and CO_{out} represent the CO concentrations (vol%) at the inlet and outlet of the gas mixture, respectively.

3. Results and Discussion

3.1. Catalyst Activity

The relationship between CO conversion and temperature is shown in Figure 1. The CO conversion increased with an increase in the temperature for all catalysts. The $\text{CuCeO}_x/\text{Fe}_2\text{O}_3$ catalyst exhibited the worst catalytic activity, and the CO conversion at 160 °C was only 62.3%. It could be seen that the performance of the $\text{CuCeO}_x/\text{Fe}_2\text{O}_3$ catalyst improved significantly after it was modified by KMnO_4 . The CO conversion initially increased with an increase in the concentration of KMnO_4 , and then it decreased. The $\text{CuCeO}_x\text{-7K}/\text{Fe}_2\text{O}_3$ catalyst showed the highest activity, corresponding to 47.9% and 85.1% CO conversion at 80 °C and 160 °C, respectively. By further increasing the concentration to 0.1 mol/L, the CO conversion at 160 °C decreased to 78.2% for the $\text{CuCeO}_x\text{-9K}/\text{Fe}_2\text{O}_3$ catalyst, which may be due to the fact that effective active sites were covered by excessive Mn species.

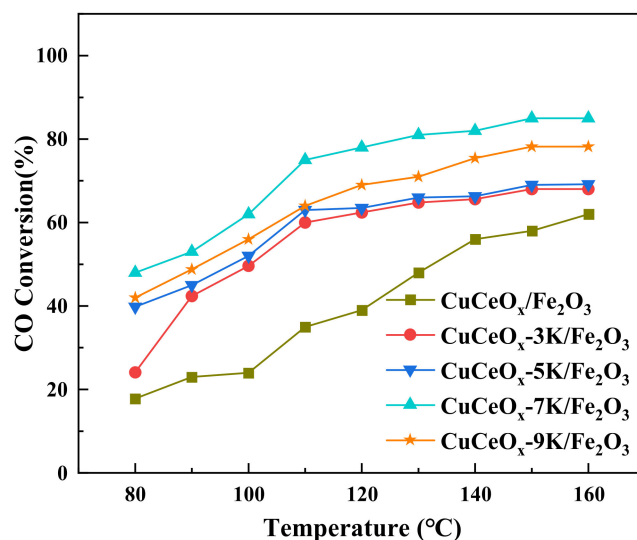


Figure 1. CO conversion of $\text{CuCe-xK}/\text{Fe}_2\text{O}_3$ catalysts.

3.2. Structural and Textural Properties

3.2.1. XRD Analysis

The XRD patterns of the catalysts are shown in Figure 2. The $\text{CuCeO}_x\text{-xK}/\text{Fe}_2\text{O}_3$ catalyst mainly presented the diffraction peaks of the Fe_2O_3 hematite phase at 24.07° , 33.14° , 35.53° , 40.98° , 49.52° , and 54.14° . The weak diffraction peaks at 32.1° , 35.50° , 38.73° , and 48.8° could be attributed to the presence of CuO . CeO_2 diffraction peaks in the catalyst appeared at 28.59° , 33.02° , and 47.4° . The cubic fluorite-type structure of CeO_2 did not change during calcining. It could be seen that the intensities of the diffraction peaks of CuO and CeO_2 were low, indicating that Cu and Ce species were highly dispersed on Fe_2O_3 . In addition, the intensities of the diffraction peaks of the metal oxides were weaker after KMnO_4 modification. According to the Scherrer formula, $L = K\lambda/\beta \cdot \cos\theta$, this could indicate that the sizes of the active particles decreased, confirming that the growth of the particles was inhibited by KMnO_4 modification. No diffraction peak related to Mn species was observed. The possible reasons for this are as follows: a high dispersion with a small size, low crystallinity, the formation of a solid solution, a low Mn content, and/or a mixture of these. The unit cell parameter a_0 was calculated for the different catalysts, and the results are listed in Table 1. It could be observed that the unit cell parameter a_0 of the catalysts decreased after they were modified with KMnO_4 .

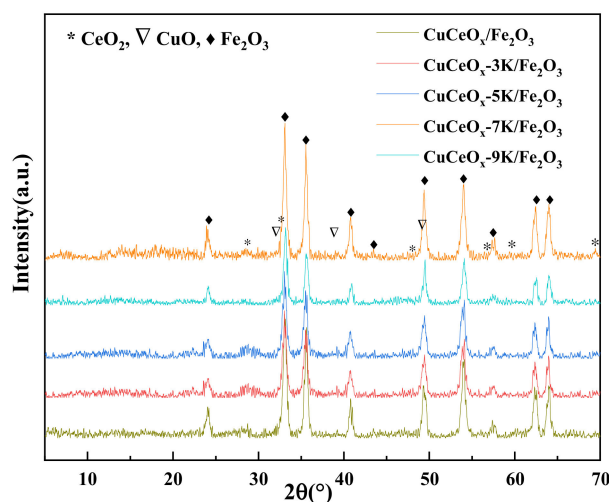


Figure 2. XRD patterns of the $\text{CuCeO}_x\text{-xK}/\text{Fe}_2\text{O}_3$ catalysts.

3.2.2. BET Analysis

According to the linear classification of the adsorption isotherm by IUPAC [21], it could be judged that the N_2 adsorption/desorption isotherms of the $\text{CuCeO}_x\text{-xK}/\text{Fe}_2\text{O}_3$ catalyst in Figure 3 belong to type IV. Moreover, the monolayer adsorption stage of this linear type appeared at the relative pressure. The adsorption curves were separated from the desorption curves at a higher relative pressure, and the rate of change of the curve gradually became gentle. When the relative pressure was close to the saturated vapor pressure, the curves increased due to the adsorption of macropores. Moreover, there was a relatively hysteric loop in the relative pressure range of 0.45~0.95, which was a typical mesoporous adsorption isotherm, and the desorption isotherm failed to coincide, indicating that the sample contained a large number of mesopores.

It is worth noting that catalytic activity is closely related to the specific surface area and pore size due to the adsorption and diffusion of reactant molecules and products. The corresponding BET surface area and the total pore volume of the $\text{CuCeO}_x\text{-xK}/\text{Fe}_2\text{O}_3$ catalysts are summarized in Table 3. The specific surface area and pore volume of the $\text{CuCeO}_x\text{-xK}/\text{Fe}_2\text{O}_3$ catalyst decreased with an increase in the KMnO_4 concentration, while the pore size showed the opposite trend. With an increase in the KMnO_4 concentration from 0.03 mol/L to 0.9 mol/L, the specific surface area decreased from $35 \text{ m}^2/\text{g}$ to $27 \text{ m}^2/\text{g}$,

and the pore volume decreased from 0.070 m³/g to 0.061 m³/g. The strong oxidation property of KMnO₄ cleared the impurities in the pore channels of the catalyst, resulting in the increase in the pore size, while some Mn species entered the pore channels, reducing the specific surface area and pore volume of the catalyst.

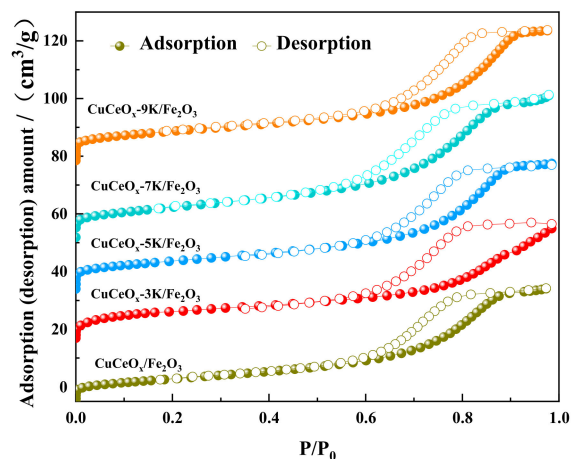


Figure 3. The N₂ adsorption/desorption isotherms of CuCeO_x-xK/Fe₂O₃ catalysts.

Table 3. The pore structure properties of the CuCe-xK/Fe₂O₃ catalyst.

| Samples | S _g (m ² /g) | V _p (m ³ /g) | Pore Size (nm) |
|---|------------------------------------|------------------------------------|----------------|
| CuCeO _x /Fe ₂ O ₃ | 36 | 0.076 | 8.022 |
| CuCeO _x -3K/Fe ₂ O ₃ | 35 | 0.070 | 7.774 |
| CuCeO _x -5K/Fe ₂ O ₃ | 33 | 0.067 | 7.786 |
| CuCeO _x -7K/Fe ₂ O ₃ | 29 | 0.064 | 7.936 |
| CuCeO _x -9K/Fe ₂ O ₃ | 27 | 0.061 | 8.395 |

3.2.3. SEM Analysis

The SEM images of the CuCeO_x-xK/Fe₂O₃ catalysts are shown in Figure 4. It can be seen in Figure 4a that the surface of CuCeO_x/Fe₂O₃ was smooth. In Figure 4b–d, it can be seen that the surface of the catalysts became rough with an increase in the KMnO₄ concentration. Moreover, the active particles were highly dispersed on Fe₂O₃ with a small size. This may be due to the strong oxidation of KMnO₄ resulting in the formation of more defects on the surface of Fe₂O₃, which was conducive to the anchoring of active particles, subsequently promoting dispersion.

3.2.4. Raman Analysis

The Raman spectrum of the CuCeO_x-xK/Fe₂O₃ catalysts is shown in Figure 5. Vibration peaks appeared at 227 cm⁻¹, 246 cm⁻¹, 296 cm⁻¹, 411 cm⁻¹, 498 cm⁻¹, 611 cm⁻¹, and 661 cm⁻¹, which match the characteristic peak of Fe₂O₃. Among them, the peaks at 227 cm⁻¹ and 498 cm⁻¹ correspond to the A_{1g} vibrational mode. The peaks at 246 cm⁻¹, 296 cm⁻¹, 411 cm⁻¹, and 611 cm⁻¹ correspond to the E_g vibrational mode, and the peaks at 661 cm⁻¹ are related to the disorder effect or the presence of Fe₂O₃ nanocrystals. In addition, it could be seen that the Raman peak of the catalyst around 661 cm⁻¹ moved to the low wavenumber of 658 cm⁻¹, indicating that the interaction between Cu and Ce could be strengthened by the addition of potassium permanganate, thereby enhancing the liquidity of the oxygen vacancies.

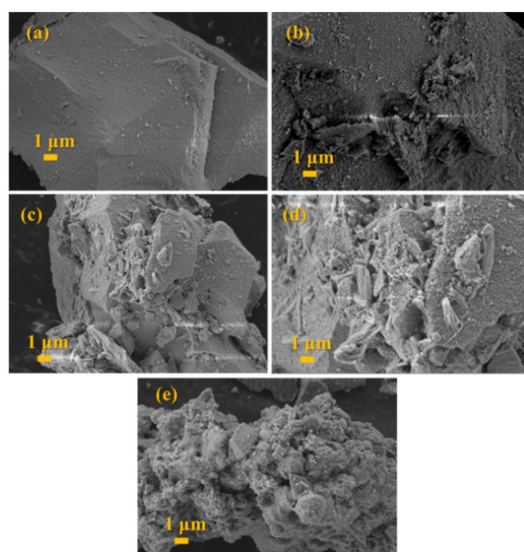


Figure 4. SEM images of $\text{CuCeO}_x/\text{Fe}_2\text{O}_3$ (a), $\text{CuCeO}_x\text{-3K}/\text{Fe}_2\text{O}_3$ (b), $\text{CuCeO}_x\text{-5K}/\text{Fe}_2\text{O}_3$ (c), $\text{CuCeO}_x\text{-7K}/\text{Fe}_2\text{O}_3$ (d), $\text{CuCeO}_x\text{-9K}/\text{Fe}_2\text{O}_3$ (e).

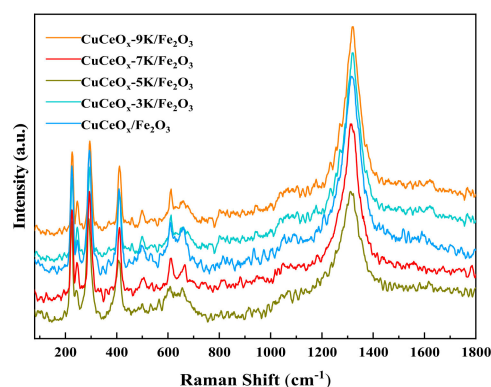


Figure 5. Raman spectrum of the $\text{CuCeO}_x\text{-xK}/\text{Fe}_2\text{O}_3$ catalysts.

3.3. Redox Properties

3.3.1. FT-IR Analysis

The FT-IR spectra of the $\text{CuCeO}_x\text{-xK}/\text{Fe}_2\text{O}_3$ catalysts are shown in Figure 6. It can be seen that the infrared spectra of the catalysts before and after KMnO_4 modification are generally consistent. No new peak appeared, indicating that the modification did not change the type of oxygen-containing functional groups. The absorptions in the spectra were attributed based on the literature [22–24]. The bands at 1400 cm^{-1} and 3416 cm^{-1} could be attributed to the H-O bending vibration in phenols and carboxyls. The peaks at 1130 cm^{-1} belong to C-O stretching vibrations. C-H stretching vibrations could be observed at 3010 cm^{-1} . The bands at 1617 cm^{-1} could be assigned to the presence of C=O stretching vibrations, which could improve the electrochemical performance by enhancing the electron transfer rate. The bands at 3128 cm^{-1} could belong to -CH, -CH₂, or -CH₃ groups. The bands at 458 cm^{-1} and 543 cm^{-1} could be assigned to the bending vibrations of metal oxides. The intensities of the peaks of oxygen-containing functional groups, such as H-O, C=O, and those on the surface of the $\text{CuCeO}_x\text{-xK}/\text{Fe}_2\text{O}_3$ catalyst, were enhanced significantly compared to those of $\text{CuCeO}_x/\text{Fe}_2\text{O}_3$, confirming that the number of oxygen-containing functional groups could be increased after KMnO_4 modification. The oxygen-containing functional groups could bind to metal particles and act as anchoring sites to prevent the aggregation of active components. In addition, oxygen-containing functional groups could serve as oxygen sources to provide reactive oxygen species for CO oxidation, directly improving catalytic activity.

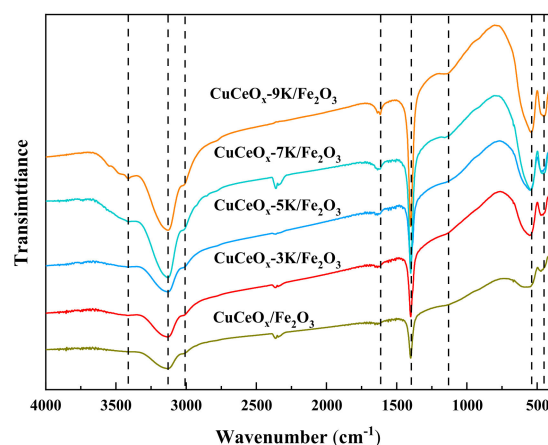


Figure 6. FT-IR profile of the $\text{CuCeO}_x\text{-xK/Fe}_2\text{O}_3$ catalysts.

3.3.2. H_2 -TPR Analysis

The redox characteristics of catalysts are also one of the main factors affecting the catalytic oxidation activity of CO. H_2 -TPR is usually used to study the redox characteristics of catalysts. As shown in Figure 7, the catalysts exhibited two reduction peaks, which were attributed to the reduction of different Cu species. The peaks at the low temperatures (α), which was 198 °C and 126 °C for $\text{CuCeO}_x/\text{Fe}_2\text{O}_3$ and $\text{CuCeO}_x\text{-7K/Fe}_2\text{O}_3$, respectively, indicate the reduction of Cu species that were highly dispersed on the catalyst surfaces. Moreover, the peaks (β) at 257 °C and 217 °C for $\text{CuCeO}_x/\text{Fe}_2\text{O}_3$ and $\text{CuCeO}_x\text{-7K/Fe}_2\text{O}_3$, respectively, could be attributed to the reduction of Cu species in the strong interaction of the Cu- O_x -Ce structure. According to the previous literature [25], the reduction of pure CuO occurs at 380 °C, which is higher than the reduction of Cu species over $\text{CuCeO}_x/\text{Fe}_2\text{O}_3$. This may have been due to the formation of interactions between Cu-Ce-Fe-O oxides, which facilitate the reduction performance. It could be seen that both the α and β of $\text{CuCeO}_x\text{-7K/Fe}_2\text{O}_3$ shifted to a lower temperature than those of $\text{CuCeO}_x/\text{Fe}_2\text{O}_3$, confirming that the reduction performance of the catalysts could be improved by the KMnO_4 modification. This may have been due to the trace Mn species resulting from the beneficial synergistic effect with CuO, CeO_2 , and Fe_2O_3 , which promoted the reduction of Cu species. In addition, the area of β for $\text{CuCeO}_x\text{-7K/Fe}_2\text{O}_3$ was much larger than that for $\text{CuCeO}_x/\text{Fe}_2\text{O}_3$, proving that the interaction between Cu and Ce was enhanced after the modification to form more Cu- O_x -Ce species. The $\text{CuCeO}_x\text{-7K/Fe}_2\text{O}_3$ catalyst with a greater number of Cu- O_x -Ce species exhibited higher activity, indicating that the Cu- O_x -Ce species were more active structures than the highly dispersed Cu species, consistent with the previous research [14,26,27]. No reduction peak of manganese oxide was observed, which may be due to the low Mn content.

3.3.3. CO-TPD Analysis

In Figure 8, it can be seen that the CO molecules could react with reactive oxygen species only after being adsorbed at the active sites and activated. Therefore, CO adsorption is the key step in the reaction. It can be seen in Figure 8 that there is a narrow desorption peak at 100~200 °C and a broad desorption peak at 250~550 °C for the $\text{CuCeO}_x\text{-xK/Fe}_2\text{O}_3$ catalyst, which are related to different CO adsorption modes. According to previous research [28], part of CO combines with lattice oxygen to form surface carbonates at low temperatures, and it then breaks down and releases CO_2 . Another part of CO reacts with lattice oxygen to generate bidentate carbonate, which decomposes into CO_2 at higher temperatures. The peak of the $\text{CuCeO}_x\text{-xK/Fe}_2\text{O}_3$ catalyst exhibited a large area, which proved that there were a large number of CO adsorption active sites on the surface. In addition, the low desorption peak temperature indicates that the decomposition of carbonate species was easy on $\text{CuCeO}_x\text{-xK/Fe}_2\text{O}_3$.

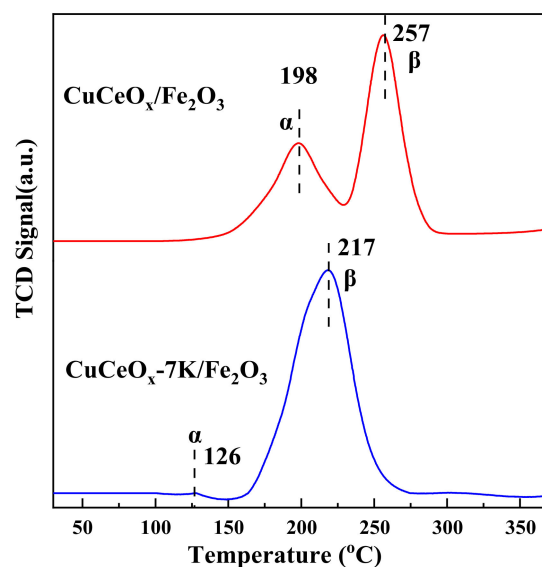


Figure 7. H_2 -TPR spectrum of $CuCeO_{x-xK}/Fe_2O_3$ catalysts.

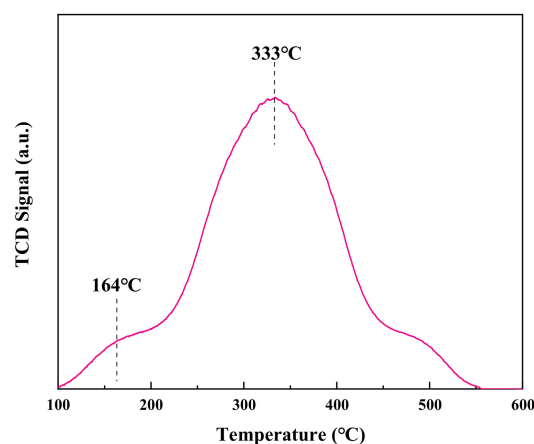


Figure 8. CO-TPD profile of $CuCeO_{x-xK}/Fe_2O_3$ catalyst.

4. Conclusions

A $CuCeO_x/Fe_2O_3$ catalyst was modified by $KMnO_4$ to remove CO in industrial flue gas. The $CuCe-7KMn/Fe_2O_3$ catalyst modified with $KMnO_4$ at a concentration of 0.07 mol/L obtained the highest activity, which corresponded to 85.1% CO conversion at 160 °C.

- (1) The modification of $KMnO_4$ inhibited the growth of the particles and promoted the uniform dispersion of the active components.
- (2) The number of oxygen-containing functional groups increased after $KMnO_4$ modification, which could provide anchoring sites for metal oxides and provide reactive oxygen species for CO oxidation as an oxygen source.
- (3) The $KMnO_4$ modification improved the redox performance of the catalyst and increased the number of active sites for CO adsorption.

Author Contributions: Conceptualization, X.X. and M.L.; methodology, L.F.; software, H.Z.; validation, L.F. and H.Z.; formal analysis, Y.D.; investigation, Z.S.; resources, Z.S.; data curation, L.Y.; writing—original draft preparation, L.F.; writing—review and editing, X.X.; visualization, Y.D.; supervision, L.Y.; funding acquisition, M.L. All authors have read and agreed to the published version of the manuscript.

Funding: This research was funded by the Special Research Project of Shanxi Provincial Education Department (No.21JK0739, No.22JK0442).

Institutional Review Board Statement: Not applicable.

Informed Consent Statement: Not applicable.

Data Availability Statement: Not applicable.

Conflicts of Interest: The authors declare that they have no known competing financial interests or personal relationships that could have appeared to influence the work reported in this paper.

References

1. Tang, X.; Wang, J.; Ma, Y.; Li, J.; Zhang, X.; Liu, B. Low-temperature and stable CO oxidation of $\text{Co}_3\text{O}_4/\text{TiO}_2$ monolithic catalysis. *Chin. Chem. Lett.* **2021**, *32*, 48–52. [[CrossRef](#)]
2. Waqas, M.; Kouotou, P.M.; El Kasmi, A.; Wang, Y.; Tian, Z.Y. Role of copper grid mesh in the catalytic oxidation of CO over one-step synthesized Cu-Fe-Co ternary oxides thin film. *Chin. Chem. Lett.* **2020**, *31*, 1201–1206. [[CrossRef](#)]
3. Xu, Z.; Yin, Q.; Li, X.; Meng, Q.; Xu, L.; Lv, B.; Zhang, G. Self-assembly of a highly stable and active $\text{Co}_3\text{O}_4/\text{H-TiO}_2$ bulk heterojunction with high-energy interfacial structures for low temperature CO catalytic oxidation. *Catal. Sci. Technol.* **2020**, *10*, 8374–8382. [[CrossRef](#)]
4. Rastegarpanah, A.; Rezaei, M.; Meshkani, F.; Dai, H. 3D ordered honeycomb-shaped CuO center dot Mn_2O_3 : Highly active catalysts for CO oxidation. *Mol. Catal.* **2020**, *485*, 110820. [[CrossRef](#)]
5. Chen, L.; Ren, S.; Xing, X.; Yang, J.; Li, J.; Yang, J.; Liu, Q. Effect of MnO_2 crystal types on $\text{CeO}_2/\text{MnO}_2$ oxides catalysts for low-temperature NH_3 -SCR. *J. Environ. Chem. Eng.* **2022**, *10*, 108239. [[CrossRef](#)]
6. Huang, J.; Teng, Z.; Kang, R.; Bin, F.; Wei, X.; Hao, Q.; Hui, K.N.; Hui, K.S.; Dou, B. Study on activity, stability limit and reaction mechanism of CO self-sustained combustion over the LaMnO_3 , $\text{La}_{0.9}\text{Ce}_{0.1}\text{MnO}_3$ and $\text{La}_{0.9}\text{Sr}_{0.1}\text{MnO}_3$ perovskite catalysts using sugar agent. *Fuel* **2021**, *292*, 120289. [[CrossRef](#)]
7. AlKetbi, M.; Polychronopoulou, K.; Jaoude, M.A.; Vasiliades, M.A.; Sebastian, V.; Hinder, S.J.; Baker, M.A.; Zedan, A.F.; Efstathiou, A.M. Cu-Ce-La-O_x as efficient CO oxidation catalysts: Effect of Cu content. *Appl. Surf. Sci.* **2020**, *505*, 144474. [[CrossRef](#)]
8. Zhang, Z.; Fan, L.; Liao, W.; Zhao, F.; Tang, C.; Zhang, J.; Feng, M.; Lu, J.Q. Structure sensitivity of CuO in CO oxidation over CeO_2 -CuO/Cu₂O catalysts. *J. Catal.* **2022**, *405*, 333–345. [[CrossRef](#)]
9. Mariño, F.; Iglesias, I.; Baronetti, G.; Alemany, L.; Laborde, M. Egg-shell CuO/CeO₂/Al₂O₃ catalysts for CO preferential oxidation. *Int. J. Hydrogen Energy* **2015**, *40*, 11235–11241. [[CrossRef](#)]
10. Reis, C.G.; Almeida, K.A.; Silva, T.F.; Assaf, J.M. CO preferential oxidation reaction aspects in a nanocrystalline CuO/CeO₂ catalysts. *Catal. Today* **2020**, *344*, 124–128. [[CrossRef](#)]
11. Xia, Y.; Lao, J.; Ye, J.; Cheng, D.G.; Chen, F.; Zhan, X. Role of Two-Electron Defects on the CeO₂ Surface in CO Preferential Oxidation over CuO/CeO₂ Catalysts. *ACS Sustain. Chem. Eng.* **2019**, *7*, 18421–18433. [[CrossRef](#)]
12. Zhu, C.; Ding, T.; Gao, W.; Ma, K.; Tian, Y.; Li, X. CuO/CeO₂ catalysts synthesized from Ce-Uio-66 metal-organic framework for preferential CO oxidation. *Int. J. Hydrogen Energy* **2017**, *42*, 17457–17465. [[CrossRef](#)]
13. Cheng, X.; Zhang, X.; Su, D.; Wang, Z.; Chang, J.; Ma, C. NO reduction by CO over copper catalyst supported on mixed CeO₂ and Fe₂O₃: Catalyst design and activity test. *Appl. Catal. B Environ.* **2018**, *239*, 485–501. [[CrossRef](#)]
14. Wang, W.W.; Du, P.P.; Zou, S.H.; He, H.Y.; Wang, R.X.; Jin, Z.; Shi, S.; Huang, Y.Y.; Si, R.; Song, Q.S.; et al. Highly Dispersed Copper Oxide Clusters as Active Species in Copper-Ceria Catalyst for Preferential Oxidation of Carbon Monoxide. *ACS Catal.* **2015**, *5*, 2088–2099. [[CrossRef](#)]
15. Wang, J.; Han, C.; Gao, X.; Lu, J.; Wan, G.; He, D.; Chen, R.; Chen, K.; He, S.; Luo, Y. Rapid synthesis of Fe-doped CuO-Ce_{0.8}Zr_{0.2}O₂ catalysts for CO preferential oxidation in H₂-rich streams: Effect of iron source and the ratio of Fe/Cu. *J. Power Sources* **2017**, *343*, 437–445. [[CrossRef](#)]
16. Zhang, X.; Cheng, X.; Ma, C.; Wang, Z. Effects of the Fe/Ce ratio on the activity of CuO/CeO₂-Fe₂O₃ catalysts for NO reduction by CO. *Catal. Sci. Technol.* **2018**, *8*, 3336–3345. [[CrossRef](#)]
17. Lu, J.; Wang, J.; Zou, Q.; He, D.; Zhang, L.; Xu, Z.; He, S.; Luo, Y. Unravelling the Nature of the Active Species as well as the Doping Effect over Cu/Ce-Based Catalyst for Carbon Monoxide Preferential Oxidation. *ACS Catal.* **2019**, *9*, 2177–2195. [[CrossRef](#)]
18. Shang, R.; Duan, Y.; Zhong, X.; Xie, W.; Luo, Y.; Huang, L. Formic Acid Modified Co_3O_4 -CeO₂ Catalysts for CO Oxidation. *Catalysts* **2016**, *6*, 48. [[CrossRef](#)]
19. Tian, Z.; Wang, C.; Si, Z.; Ma, L.; Chen, L.; Liu, Q.; Zhang, Q.; Huang, H. Fischer-Tropsch synthesis to light olefins over iron-based catalysts supported on KMnO_4 modified activated carbon by a facile method. *Appl. Catal. A Gen.* **2017**, *541*, 50–59. [[CrossRef](#)]
20. Wang, D.; Zhou, X.; Ji, J.; Duan, X.; Qian, G.; Zhou, X.; Chen, D.; Yuan, W. Modified carbon nanotubes by KMnO_4 supported iron Fischer-Tropsch catalyst for the direct conversion of syngas to lower olefins. *J. Mater. Chem. A* **2015**, *3*, 4560–4567. [[CrossRef](#)]
21. Wu, Y.; Dong, L.; Li, B. Effect of iron on physicochemical properties: Enhanced catalytic performance for novel Fe₂O₃ modified CuO/Ti_{0.5}Sn_{0.5}O₂ in low temperature CO oxidation. *Mol. Catal.* **2018**, *456*, 65–74. [[CrossRef](#)]

22. Zhang, J.; Xin, B.; Shan, C.; Zhang, W.; Dionysiou, D.D.; Pan, B. Roles of oxygen-containing functional groups of O-doped g-C₃N₄ in catalytic ozonation: Quantitative relationship and first-principles investigation. *Appl. Catal. B-Environ.* **2021**, *292*, 120155. [[CrossRef](#)]
23. Pan, Z.; Wang, K.; Wang, Y.; Tsiakaras, P.; Song, S. In-situ electrosynthesis of hydrogen peroxide and wastewater treatment application: A novel strategy for graphite felt activation. *Appl. Catal. B-Environ.* **2018**, *237*, 392–400. [[CrossRef](#)]
24. Zheng, J.; Xing, X.; Pang, Z.; Wang, S.; Du, Y.; Lv, M. Effect of Na₂CO₃, HF, and CO₂ Treatment on the Regeneration of Exhausted Activated Carbon Used in Sintering Flue Gas. *ACS Omega* **2021**, *6*, 25762–25771. [[CrossRef](#)]
25. Shen, Z.; Xing, X.; Pang, Z.; Wang, S.; Lv, M.; Jiang, X. Low Temperature CO Oxidation in Sintering Flue Gas Over Cu-Ce/AC Catalysts: Effect of Pretreatment with KMnO₄ on Activity. *Catal. Lett.* **2022**, *7*, 10502. [[CrossRef](#)]
26. Gu, D.; Jia, C.J.; Bongard, H.; Spliethoff, B.; Weidenthaler, C.; Schmidt, W.; Schüth, F. Ordered mesoporous Cu–Ce–O catalysts for CO preferential oxidation in H₂-rich gases: Influence of copper content and pretreatment conditions. *Appl. Catal. B Environ.* **2014**, *152–153*, 11–18. [[CrossRef](#)]
27. Li, L.; Han, W.; Zhang, J.; Lu, G.; Tang, Z. Controlled pore size of 3D mesoporous Cu-Ce based catalysts and influence of surface textures on the CO catalytic oxidation. *Microporous Mesoporous Mater.* **2016**, *231*, 9–20. [[CrossRef](#)]
28. Luo, Z.; Mao, D.; Shen, W.; Zheng, Y.; Yu, J. Preparation and characterization of mesostructured cellular foam silica supported Cu-Ce mixed oxide catalysts for CO oxidation. *RSC Adv.* **2017**, *7*, 9732–9743. [[CrossRef](#)]

Disclaimer/Publisher’s Note: The statements, opinions and data contained in all publications are solely those of the individual author(s) and contributor(s) and not of MDPI and/or the editor(s). MDPI and/or the editor(s) disclaim responsibility for any injury to people or property resulting from any ideas, methods, instructions or products referred to in the content.